ELSEVIER

Contents lists available at ScienceDirect

Earth and Planetary Science Letters

journal homepage: www.elsevier.com/locate/epsl





The role of fault structural evolution on long-term slip rates and seismic cycles in the Himalayan orogenic wedge

Sharadha Sathiakumar a,b,*, Sylvain Barbot a, Judith Hubbard b,c

- ^a University of Southern California, Los Angeles, USA
- ^b Earth Observatory of Singapore, Singapore
- ^c Cornell University, USA

ARTICLE INFO

Editor: J.-P. Avouac

Dataset link: https:// zenodo.org/record/4679513

Dataset link: https:// doi.org/10.5281/zenodo.10634752

Keywords: fault-bend fold shortening rates orogenic wedge mountain-building seismic cycle simulations Nepal Himalayas

ABSTRACT

The collision between the Indian and Eurasian plates drives tectonic uplift and evolving landscapes over geological time scales. Much of this evolution is accommodated by seismic processes. However, the relationship between long-term geological processes and short-term seismic cycles is challenging to unravel because of their disparate spatial and temporal scales. Here, we investigate the impact of the internal dynamics of the orogenic wedge on the cycle of Himalayan earthquakes, linking structural models with seismic cycle simulations to show how earthquake patterns may have changed over time. Balanced cross-sections with fault-bend folding at different stages of structural evolution show that frontal thrusts in the Himalayas accumulate slip at different rates across the wedge and over time, depending on the architectural layout of the thrust sheet. Along-strike variations in structural evolution along the Himalayan front may lead to lateral and down-dip segmentation of long-term slip rate, affecting the magnitude and recurrence patterns of earthquakes. Spatio-temporal earthquake patterns may shift every ~0.3-1.3 Myr as the hanging wall evolves, with implications for seismic hazards in the Nepal Himalayas.

1. Introduction

During the past 60 million years, the Indian plate has been gradually colliding with the Eurasian plate, leading to the closure of the Tethys Sea and the uplift of the Himalayan mountains to elevations of about 5 to 8 kilometers above sea level (Powell and Conaghan, 1973; Molnar and Tapponnier, 1975; Tapponnier and Molnar, 1977; Tapponnier et al., 1986, 2001; Avouac, 2003; Ding et al., 2022; Wang and Barbot, 2023). Over geological time scales spanning millions of years, the structure of the Himalayan megathrust continuously changes and impacts tectonic uplift and landscape evolution (Molnar and Tapponnier, 1975; Wesnousky et al., 1999; Yin and Harrison, 2000; Lavé and Avouac, 2000, 2001; Hubbard et al., 2016). At shorter timescales spanning seconds to thousands of years, the system features cycles of earthquakes of varying magnitudes repeating over years, centuries, and millennia (Feldl and Bilham, 2006; Bilham, 2019; Mugnier et al., 2013; Sapkota et al., 2013; Gupta and Gahalaut, 2014; Bollinger et al., 2014; Oiu et al., 2016; Wesnousky, 2020). A general question that animates the tectonophysics community is the relationship between the mountain

building process and seismic cycles (e.g., Masek and Duncan, 1998; Dal Zilio et al., 2021; Lamb, 2021; Mallick et al., 2021). Although long-term processes such as duplexing, ramp breaks, and splay faulting are known to occur within orogenic wedges (Suppe, 1983; Qiu and Barbot, 2022), and the cumulative effect of incremental slip during and between earthquakes is to raise mountains (Darwin, 1840), these phenomena are challenging to incorporate in models of seismic cycles because of the disparate spatial and temporal scales involved (Van Dinther et al., 2013; Van Zelst et al., 2019; Dal Zilio et al., 2019; Petrini et al., 2020; Uphoff et al., 2023).

Here, we investigate how strain is partitioned between slip on the Himalayan megathrust and internal deformation of the hanging wall, leading to the creation of permanent topography, and how the structural complexity of the mechanical system affects short-term seismic cycles in the Nepalese Himalayas. We explore the structural evolution of the megathrust along two representative cross-sections in Central Nepal (CN) and East Nepal (EN) that feature distinct degrees of structural complexity. We build kinematic structural models that account for

^{*} Corresponding author at: Earth Observatory of Singapore, Singapore. *E-mail address:* sharadhask03@gmail.com (S. Sathiakumar).

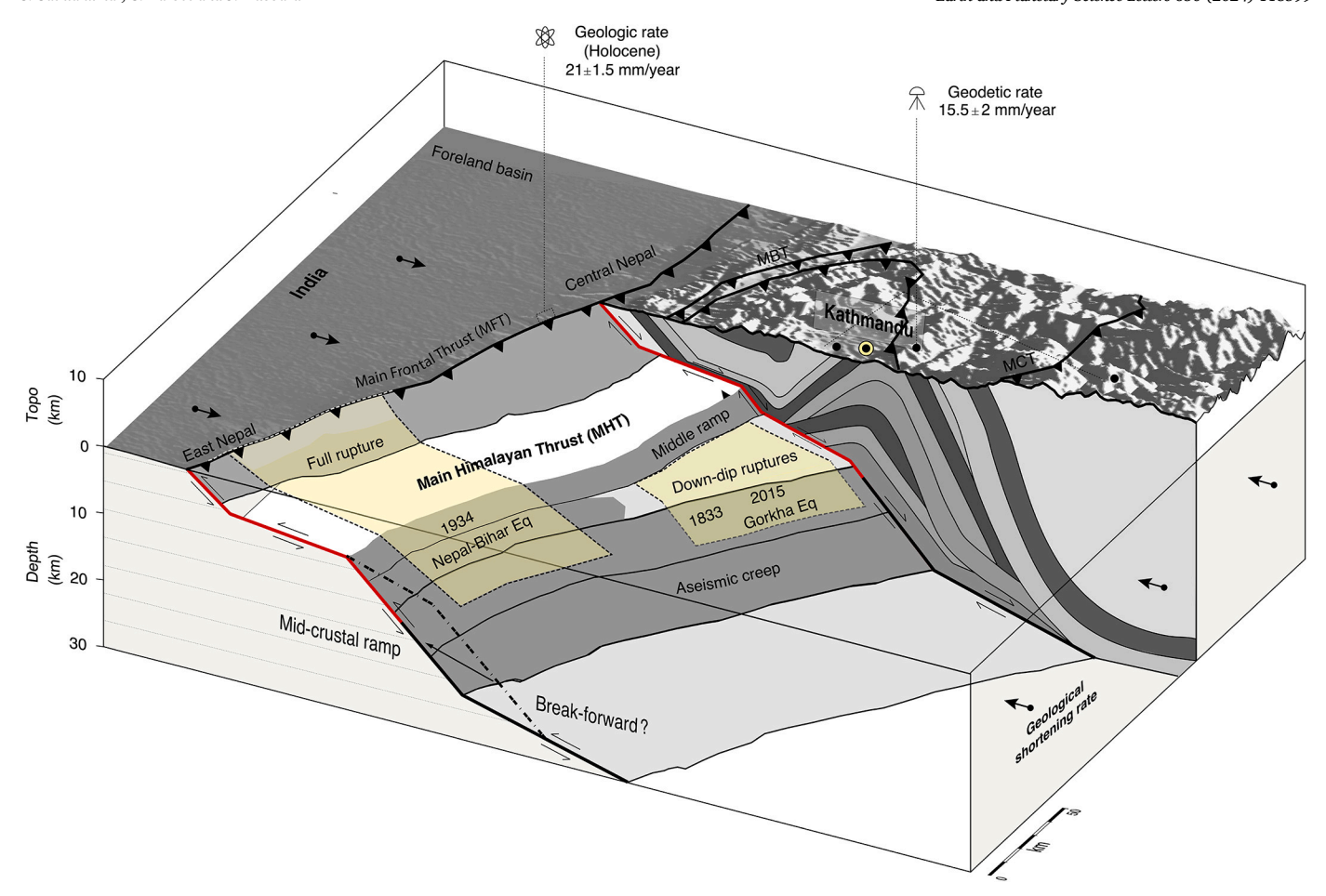


Fig. 1. Perspective view of the Himalayan subsurface and observational constraints on the shortening-rate in Nepal. The three-dimensional fault geometry with 3x vertical exaggeration and the cross-sectional surface across Central Nepal are plotted based on Hubbard et al. (2016). The fault geometry at two representative cross-sections in Central and East Nepal (CN and EN, respectively) is highlighted with the frictionally unstable seismogenic zone in red and the creeping region in black. The contours for the last known earthquakes in these segments, the M_w 8.2 1934 Nepal-Bihar earthquake (EN) and the M_w 7.8 2015 Gorkha earthquake (CN), are represented in yellow. Dashed lines along the Main Frontal Thrust (MFT) indicate the surface trace of the 1934 event, as widespread evidence of surface rupture along the entire length is challenging to discern (Sapkota et al., 2013; Bollinger et al., 2014; Wesnousky et al., 2018; Rizza et al., 2019; Riesner et al., 2023). Central Nepal features a middle ramp that is absent in East Nepal. Fault system evolution allows break-forward episodes of one or more ramps allowing accretion of Indian lithosphere onto the upper plate. The long-term geological shortening rate spanning multiple seismic cycles is shown with arrows. The local long-term slip on individual fault segments, which may vary down-dip due to internal deformation of the orogenic wedge, is represented by double arrows.

the internal deformation of the orogenic wedge by active folding in the hanging wall and underplating in the footwall of the Main Himalayan Thrust (MHT). We show that strain can be stored and released in the hanging wall at timescales of millions of years during stages of uplift and duplexing, producing dynamic segmentation of the long-term slip rate down-dip and along the megathrust, with possibly distinct geologic and geodetic slip rates. Using numerical simulations of seismic cycles with active folding, we show how the internal deformation of the hanging wall can lead to different spatio-temporal patterns of earthquake cycles and corresponding seismic hazards.

2. Architecture and structural development of the Himalayan orogenic wedge

The Himalayan orogenic wedge consists of a forward-propagating sequence of thrust faults; from north to south, these are the Main Central Thrust (MCT), the Main Boundary Thrust (MBT), and the Main Frontal Thrust (MFT, the most active splay fault in the system), respectively. These splay faults sole at depth into the Main Himalayan Thrust (MHT), which accommodates crustal shortening and related deformation (Fig. 1). The base of the MHT consists of a mid-crustal ramp, a steeply dipping thrust fault segment that connects two levels of décollement (gently dipping, bed-parallel thrust fault). Slip along this ramp

influences the long-term uplift of Himalayan rocks, as well as short-term seismicity due to persistent strain accumulation (Avouac, 2003; Hubbard et al., 2016; Dal Zilio et al., 2021).

In Central Nepal, the presence of a mid-crustal ramp is evidenced by seismic reflection studies (Hauck et al., 1998), microseismicity (Pandey et al., 1995), geologic data (Schelling and Arita, 1991; Hubbard et al., 2016), and magnetotelluric data (Lemonnier et al., 1999). The position of the mid-crustal ramp in East Nepal can be traced using the surface expression of Gorkha-Pokhara anticlinorium (GPA) as a proxy. The structural heterogeneity in the fault architecture is illustrated by the curvature of the GPA along strike. Another structural complexity in the MHT is the presence of a middle ramp in Central Nepal within the seismogenic zone (Hubbard et al., 2016). The middle décollement ruptured during the recent 2015 M_w 7.8 Gorkha earthquake and the 1833 rupture (Avouac et al., 2015; Bilham, 1995). Unlike areas to the east and west, Central Nepal has not experienced a megathrust-spanning full rupture (from the base of the megathrust to the surface) in the last ~ 800 years, indicating that strain remains to be released and suggesting an impending seismic hazard (Bollinger et al., 2016). This middle décollement, however, vanishes to the east, as the ramps below and above it merge into a single large mid-crustal ramp (Hubbard et al., 2016). The last known earthquake to rupture this section of Nepal is the 1934 Nepal-Bihar earthquake (Pandey and Molnar, 1988).

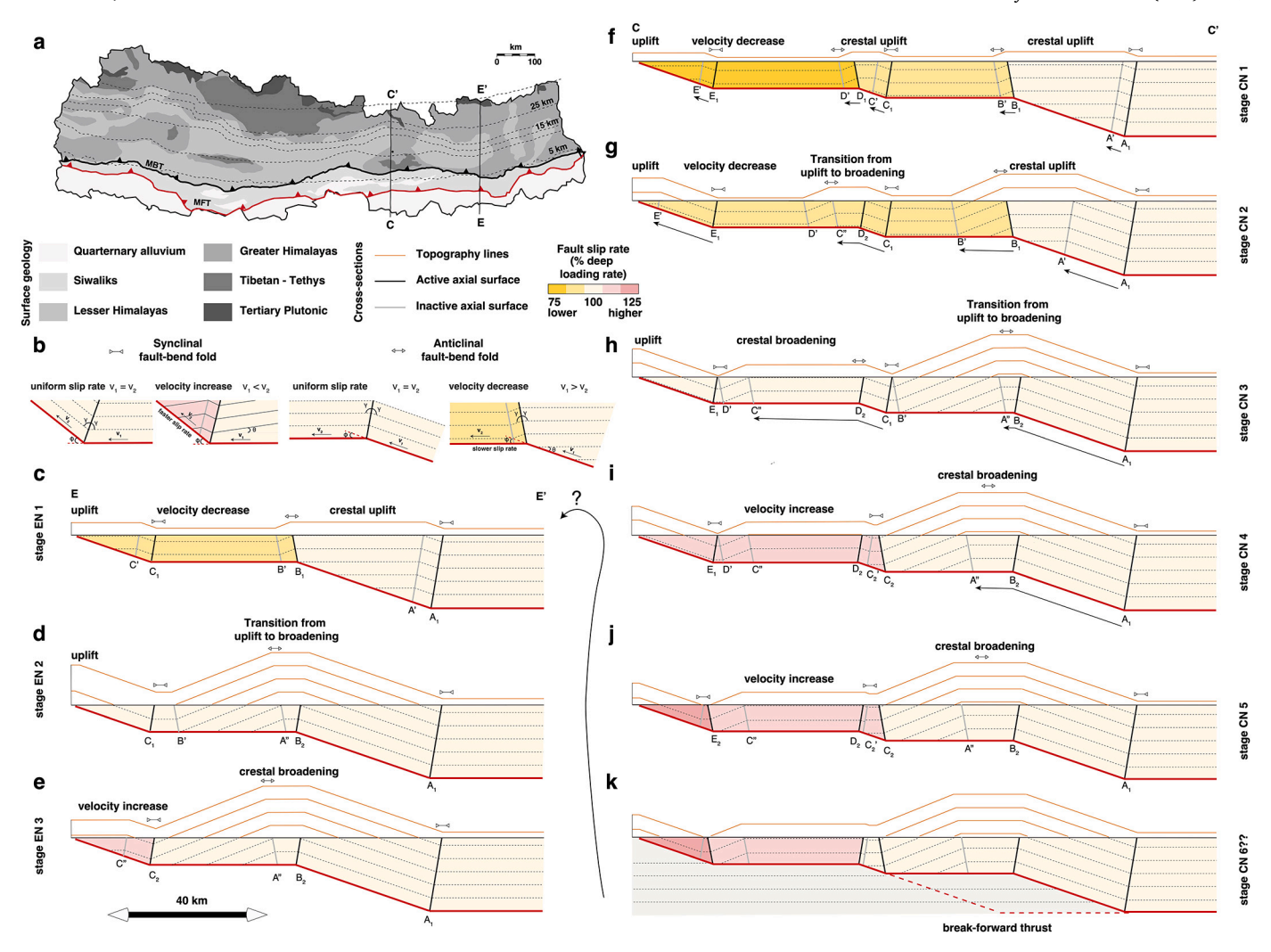


Fig. 2. Structural evolution of the MHT in Central and East Nepal. a) The locations of the two-dimensional profiles in Central (CC') and East (EE') Nepal are shown on a geological map of Nepal. b) Illustration of fault-bend fold theory concepts applied to reconstruct the structural development of the Himalayan megathrust. The long-term slip rate of fault segments varies depending on the fold shape and the history of deformation. The Main Frontal Thrust (MFT) can slip at a rate faster (pink) or slower (yellow) than the long-term loading rate due to active folding and shortening. Reconstruction of hanging wall evolution along profile EE' in East Nepal (c-e) and profile CC' in Central Nepal (f-k).

To explore the evolution of the fault system and its impact on the earthquake cycle, we use representative two-dimensional cross-sections along Central and East Nepal with variations in down-dip fault geometry. We apply quantitative models of fault-bend folding to study the geometric and kinematic development of folds, and create a sequence of cross-sections that illustrate the structural evolution of the hanging wall as shortening progresses, paying particular attention to the long-term slip rates on different fault segments. Following standard fault-bend folding methods, we hold the thickness of stratigraphy across each fold and the cross-sectional area constant (Suppe, 1983). We model axial surfaces or fold axes as infinitesimally narrow, approximating the small thickness of fault and stratigraphic bends relative to the 200-km length scale of the plate boundary (Sathiakumar et al., 2020).

Large anticlines, like the GPA, are created due to slip across composite fault bends with a flat-ramp-flat geometry. When stratigraphic layers traverse fault bends, they are folded and uplifted, building topography. Notably, when these layers are at an angle to the fault, the slip magnitude on either side of the fault bend will be different, due to the geometric conservation of total cross-sectional area (Suppe, 1983; Shaw et al., 2005). In our progressive cross-sections, we track these changes in slip rate across the multiple fault bends in the MHT as shortening progresses (Fig. 2). The ratio of slip below and above the bend

depends on the shape of the fault and the associated fold (Suppe, 1983; Shaw et al., 2005).

Our two-dimensional cross-sections of Central and East Nepal (CN and EN, respectively) are based on the three-dimensional fault geometry described by Hubbard et al. (2016). In the early developmental stages (stages CN1, CN2, EN1), the stratigraphic layers are parallel to the underlying fault everywhere except above the ramps, which cut through existing layers (Fig. 2c,f,g). As the hanging walls of the ramps are pushed up, they travel over fault bends onto the shallower flat fault segments, causing folding and a change in slip rate. These types of fault bends, called anticlinal fault bends, are associated with a decrease in slip rate. In our cross sections, this implies that up-dip fault segments will have lower long-term fault slip rates compared to the deep loading rate (Fig. 2). With typical Nepal fault structure parameters, we obtain a decrease of ~12-15% (stages EN1, CN2) or ~25% (stage CN1) in frontal fault slip rate, reflecting one or two anticlinal fault bends, respectively. During these stages, the structures are in a predominantly "crestal uplift" phase, as the crests of the anticlines continue to rise, contributing to the growth of topography (Fig. 2).

As shortening continues, the kink bands widen, and the inactive axial surface associated with the base of the ramp reaches the top of the ramp. At this point, the hanging wall rocks above the ramp become parallel to the ramp, and the slip rate across the upper bend becomes

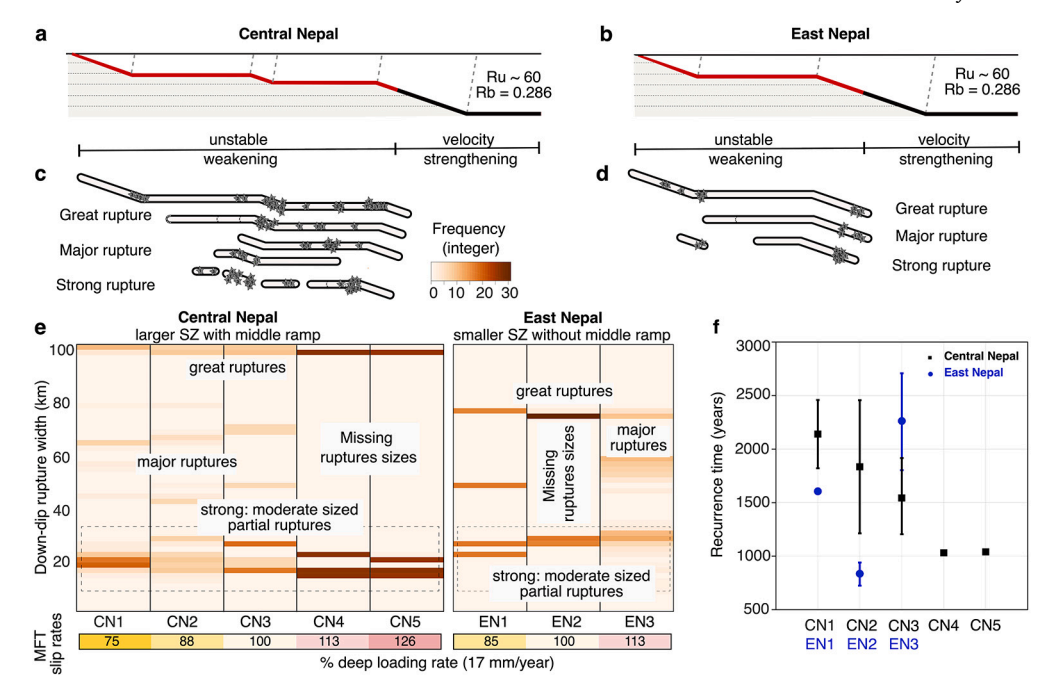


Fig. 3. Seismotectonic implications of down-dip long-term slip-rate variations. a and b) Illustrations of two-dimensional fault geometry models for Central and East Nepal with fault segments and sample active axial surfaces. Unstable weakening is denoted in red, velocity strengthening in black. Ru and Rb are non-dimensional numbers that control the dynamics of fault behavior in the rate-and-state friction framework. Ru is the ratio of seismogenic zone width to characteristic nucleation size, and Rb is the ratio of static to dynamic stress drop. c and d) Down-dip rupture width illustration for megathrust-spanning full ruptures (great ruptures), multiple-segment large ruptures (major ruptures), and single-segment ruptures (strong ruptures); stars indicate hypocenter locations. e) Colored histogram indicating frequency of ruptures of a given width for each of the stages in our simulations (CN1-CN5, EN1-EN3). Darker colors indicate more frequent ruptures. Lower bar indicates the slip rate of the MFT for each stage; colors of lower bar are taken from Fig. 2. f) Recurrence times of great ruptures for all models (black: Central Nepal stages CN1-CN5; blue: East Nepal stages EN1-EN3).

constant (stages CN3, EN2). This brings the local long-term slip rate on all the fault segments back to the deep loading rate (Fig. 2 d,h). The structural signature of this process now transitions to "crestal broadening", with passive transport of the folded kink bands along the upper detachments, and the crests of the associated anticlines grow in width but not height. In the later stages (stages CN4, CN5, EN3), inclined stratigraphic layers that already went through one folding process start to climb the up-dip ramps. The resulting folds, called "synclinal faultbend folds", are associated with an increase in slip rate on the up-dip part of the fault (Fig. 2 e,i,j). In our cross sections, this creates a $\sim 13\%$ (stages EN3, CN4) or $\sim 26\%$ (stage CN5) increase in long-term slip rate at the frontal thrust compared to the deep loading rate, reflecting one or two synclinal fault bends, respectively.

Thus, the frontal part of the megathrust can slip slower or faster than the deep loading rate, averaged across the seismic cycle. These slip rates can last for hundreds of thousands to a few million years before transitioning to a new, stable slip rate. The process described here reflects the evolution of the hanging wall over a static fault geometry. The next stage of the fault system involves breaking forward of one or several of the ramps, allowing accretion of Indian lithosphere onto the upper plate. Break forward of the mid-crustal ramp will start a new cycle of fault-bend folding (e.g. stage CN6, Fig. 2k). We do not simulate the break-forward episodes explicitly. Instead, our kinematic structural model describes the geometry before and after any break-forward happens.

In the Himalayas, these long-term folding mechanisms must impose heterogeneous long-term loading rates along different segments of the plate interface that can differ measurably from the deep loading rate. As the local loading rate affects the recurrence time and other characteristics of earthquakes (Barbot, 2019; Sathiakumar et al., 2020; Shi et al., 2020; Barbot, 2020), the structural development of the orogenic wedge will modulate the short-term seismo-tectonic behavior. In the next section, we explore numerical models of the seismic cycle that incorporate

the boundary conditions and internal deformation representative of the different stages of growth of the Himalayan orogenic wedge. We use our results to discuss the impact of off-fault deformation on seismic hazards along the Central and East Nepal representative cross-sections.

3. Earthquake cycles with spatially variable slip rate and active folding

To study the impact of folding in the orogenic wedge on the seismic cycle, we employ physics-based numerical simulations of earthquake sequences using slip-rate- and state-dependent friction coupled to internal deformation of the hanging wall across active axial surfaces (Sathiakumar et al., 2020). In order to isolate the effect of structure on the two-dimensional Central and Eastern cross-sections (see Supplementary Tables 1 and 2), we use the same effective physical properties for both models, based on earthquake sequence simulations of the 2015 M_w 7.8 Gorkha earthquake (Sathiakumar and Barbot, 2021). The transition from deep steady-state velocity-strengthening behavior to shallower unstable weakening is fixed at $\sim\!15\,\mathrm{km}$. The deep loading rate in both models is set to 17 mm per year, which is an intermediate rate between the best-fit geodetic and geologic rates, and within the uncertainty range of geodetic models.

We incorporate axial surface dynamics to account for off-fault deformation associated with fault bends. To bridge long-term (> 100,000 to a few million years) and shorter-term or seismic cycle timescales (seconds to thousands of years), we implement our kinematic forward model of the structural evolution of the hanging wall: we generate one model for each stage of development in Central and Eastern Nepal (stages CN 1-5, EN 1-3, Fig. 2, Supplementary Figure 1). For each of these models, we simulate seismic cycles for 20,000 years and compare the results to study the evolution of seismic behavior as the hanging wall deforms. For each region, the underlying fault geometry and frictional properties remain the same, while the slip rates of the fault segments and the ori-

entations of the axial surfaces within the hanging wall stratigraphy vary (Supplementary Figure 1). This model allows us to study how long-term geological evolution impacts short-term seismic processes.

We simulate super-cycles of earthquakes that express megathrust-spanning full ruptures (great ruptures), multiple-segment large ruptures that may or may not break the surface (major ruptures), and smaller ruptures that break individual fault segments (strong ruptures). Each seismic super-cycle starts and ends with a through-going "great" rupture.

Our models show that variations in slip rate impact several earth-quake cycle characteristics, including down-dip rupture width (and therefore magnitude), hypocenter location, and the recurrence times of great and partial ruptures (Supplementary Figures 2, 3). First, frontal fault slip rates impact the recurrence times of great ruptures (Fig. 3). When the frontal slip rates are higher than the deep loading rate, our models produce more frequent great events with less slip per event, compared to the more infrequent, larger events associated with slower frontal slip (mean recurrence time of $\sim 1,000$ years versus $\sim 1,800$ years, respectively). The recurrence time of great ruptures is also more periodic for faster frontal slip compared to more chaotic for slower frontal slip.

In addition to impacting the largest ruptures, long-term slip-rate variability also modifies the number of partial ruptures between two great ruptures (i.e., within a complete super-cycle). Models in which the frontal slip rate is lower or the same as the loading rate produce twice as many incomplete ruptures per super-cycle compared to those with faster frontal slip. These partial ruptures are of variable size, ranging from multi-segment major ruptures to single-segment strong ruptures. Models with faster frontal slip also do not encompass the full spectrum of rupture sizes observed for lower frontal slip rates and exhibit less variability of hypocenter locations, which cluster around fault bends in all cases (Fig. 3 and Supplementary Figure 2).

The recurrence time and behavior of single-segment "strong" ruptures bounded by ramps, a behavior seen in the 2015 Gorkha rupture in Central Nepal, are uniform throughout the earthquake cycle in all stages of structural evolution. These events nucleate at the transition between the velocity-strengthening and velocity-weakening parts of the fault (Supplementary Figure 2). These partial ruptures of the MHT can precede or succeed great ones, with inter-event times between 100 and 500 years. In general, seismic cycle properties and patterns can shift depending on the time duration of each structural configuration and can range between 300 thousand years and 1.3 million years (Figs. 3 and 4)

The structural differences between Central and East Nepal manifest as distinct characteristics of the earthquake cycle. The seismogenic width of East Nepal is smaller, reducing the size of down-dip ruptures. It also does not contain a middle ramp; this reduces the opportunity for geometric or slip rate segmentation, and we observe a more limited range of rupture sizes as a result. The fault structure and the down-dip slip-rate segmentation determine the seismo-tectonic attributes of the system (Fig. 3 and Supplementary Figure 3).

4. Slip-rate variability in the Himalayas

The deformation of the Himalayan orogenic wedge is captured by observations sensitive to variable timescales and locations. Along the MFT, faulting and folding coupled with surface processes provide important constraints on earthquake characteristics and seismic hazard in these thrust-faulted terrains (Burbank et al., 1996; Lavé and Avouac, 2001; Godard et al., 2014; Bollinger et al., 2014; Mishra et al., 2016; Rajendran and Rajendran, 2021; Ghoshal et al., 2020). A survey of the Holocene abandoned fluvial terraces perched above the Bagmati river in Central Nepal across a 20 km wide deformation zone suggests a fault slip rate of 21 ± 1.5 mm/yr in the Himalayan foreland using geometric relationships between faulting and folding (Lavé and Avouac, 2000, 2001). At this longitude, the most recent estimates of convergence from

geodesy are $\sim 20-30\%$ smaller (15 \pm 2.4 mm/yr) (Lindsey et al., 2018; Li et al., 2018). Geodetic estimates of the shortening rate vary among studies, with previously reported geodetic rates matching the Holocene shortening rates more closely (Stevens and Avouac, 2015). However, the lower rate of 15 mm/yr consistently explains the various geodetic data in Nepal (See Section 3.4 in Lindsey et al., 2018) and the total India-Tibet convergence measured in South Tibet (Zheng et al., 2017).

Considering uncertainties in the geodetic and geologic estimates of shortening rate, it is unclear whether geodetic and geologic rates truly agree or disagree locally. Additionally, longitudinal variations in strain accumulation and partitioning may play an important role (Bollinger et al., 2014; Hamahashi et al., 2022). Below, we discuss the mechanisms of deformation in the orogenic wedge that enable a possible discrepancy between geologic and geodetic shortening rates.

Fault-bend folding makes it possible for the frontal rate to exceed the deep loading rate, but only under specific conditions. In order for frontal fault slip rates to be higher than the deep loading rate in Central Nepal according to our model, the structural evolution must be in a stage similar to stages CN4, CN5, or CN6. In these stages, inclined beds are being refolded at one (CN4 and CN6) or two (CN5) additional up-dip ramps (Figs. 2 and 4).

A deep loading rate of $13-17\,\mathrm{mm/yr}$ can lead to a long-term slip rate at the frontal thrust of $14.5-19.5\,\mathrm{mm/yr}$ during stage CN4 ($\sim 13\%$ increase) and $16.5-21.5\,\mathrm{mm/yr}$ during stage CN5 ($\sim 27\%$ increase). Structural cross-sections based on surface geology at this location (Hubbard et al., 2016) suggest that the mid-crustal ramp has moved from crestal uplift to crestal broadening, and that inclined beds are climbing the up-dip middle ramp. This increases slip up-dip similar to processes described in both stages CN4 and CN5 in our models (Fig. 4a).

Our kinematic models capture the first-order approximations of fault evolution with a fixed geometry. More accurate models can capture other complexities like break-forward processes of the frontal fault system. For instance, the middle ramp originally formed as the lower part of a surface-breaching Main Boundary Thrust fault (MBT) and, eventually, its hanging wall rocks were uplifted and eroded away. Our model does not include this evolution; instead, these hanging wall rocks are transported up the fault, and in stage CN5 cause an additional increase in slip rate updip as they reach the MFT. The slip rate increase in stage CN5 is therefore not supported at this location, although intermediate ramps like this one may be active in other locations. Thus, although the possible difference in slip rate from geological and geodetic estimates in Central Nepal is best fit by stage CN5, stage CN4 is more representative.

In East Nepal, shallow slip rates remain uncertain. Data from sediments in boreholes in the Himalayan foothills reveal the deformation history and MFT fault slip rates on the Bardibas fault, the southernmost segment of the frontal thrust (Hamahashi et al., 2022). At the Bhabsi river, shortening rates are $\sim 3 - 12$ mm/yr, accommodating 20-80% of the geodetic shortening rate. This lower slip rate is due to partitioning of shortening onto other hanging wall faults, including the Patu Thrust in the north, as this is a step-over region between the two faults; incorporating this additional shortening could plausibly make the total shortening comparable to geodetic rates (Hamahashi et al., 2022). Notably, river terraces from the Ratu river, just east of the Bhabsi River suggest uplift rates of 10-12 mm/yr on the Bardibas Thrust (Bollinger et al., 2014), possibly suggesting 20-35 mm/yr of shortening assuming a $20-30^{\circ}$ dipping fault. These widely variable rates, from far below to far above the geodetic loading rate, highlight the difficulty of measuring geologic rates. In addition to structural uncertainties, non-tectonic climate signals can affect the uplift of river terraces (Hamahashi et al., 2022).

Here, we demonstrate that this budget can also vary depending on the hanging wall structure. In the case of Eastern Nepal, the total MFT shortening budget could be consistent with the lower slip rate estimate from the Bhabsi River (in stage EN1) or the higher slip rate estimate from the Ratu River (in stage EN3). Given the uncertainties in estimates and the likelihood of additional active faults and sedimentary processes,

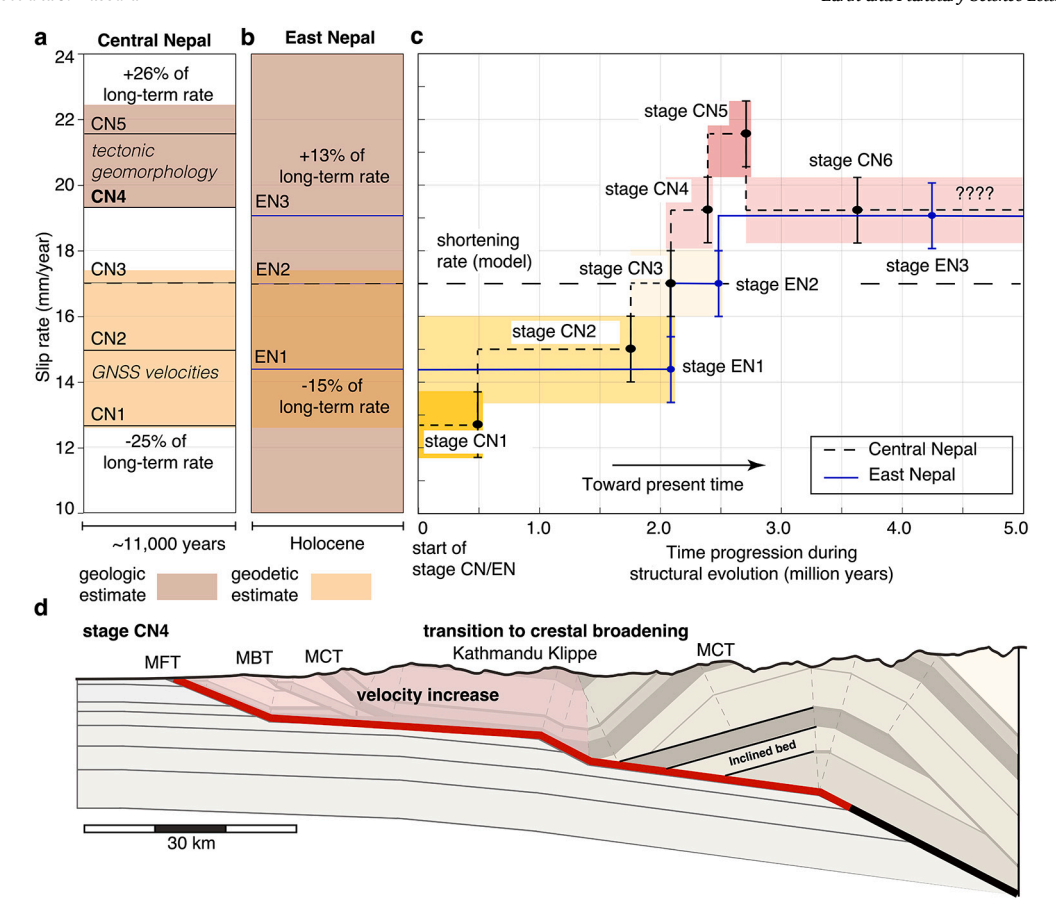


Fig. 4. Variations of long-term slip-rates on the MFT over multi-million year timescales due to active folding and duplexing compared to the geodetic loading rate. a and b) Fault-bend folding predicts different frontal fault slip rates depending on the history of kinematic development (black and blue horizontal lines representing Central and East Nepal, respectively). In Central Nepal (a) the geologic shortening rate at the MFT (estimated from fluvial terraces, indicated by the shaded brown region) is 10-30% higher than the geodetic loading rate for the MHT (shaded yellow region). An increase in frontal long-term slip rate is possible due to the uplift of inclined rock layers in Central Nepal in stages CN4-CN6. In East Nepal, the geologic rates are highly uncertain, and so it is not currently possible to distinguish between different stages of evolution based on rates alone. C) Evolution of long-term slip rate on the shallow MHT and MFT in Central Nepal (black) and East Nepal (blue). The modified slip rates due to structural evolution are sustained for many seismic super-cycles, spanning hundreds of thousands to a few million years. D) Geological cross-section of Central Nepal (Hubbard et al., 2016), showing inclined beds climbing the middle-ramp, causing a long-term slip rate increase in the up-dip segments, similar to Stage CN4.

all stages remain possible. To reduce the uncertainties of geologic rates, better assessing the detailed structure of the orogenic wedge may be particularly useful.

As mountain-building processes continue in the Himalayas, ramps break forward to create duplexes, and the system transitions to a new cycle of structural evolution. A hypothetical stage CN6 shows how southward migration of the mid-crustal ramps could shift the fault structure in Central Nepal to a setup similar to East Nepal. In all scenarios, geodetic data can estimate the long-term deep loading rate representative of the India-Eurasia convergence across the MHT, while the shallow geomorphic rates can help constrain the dynamics of the hanging wall in the toe of the orogenic wedge.

5. Discussion and conclusions

The relationship between mountain building and megathrust seismicity is poorly understood. Seismic cycles are thought to result primarily from elastic interactions. Yet, over geological time scales, the rise of mountains shows clear evidence of permanent, inelastic deformation. In fold-and-thrust belts, the internal deformation of the orogenic wedge accommodates a variable strain rate over millions of years due to active folding in the hanging wall. Off-fault strain accumulation occurs during periods of crestal uplift and is manifested by slower frontal fault slip rates. Strain release occurs during crestal broadening by speeding

up the frontal thrusts. These variable rates can be stable for 100,000 to millions of years as the orogenic wedge evolves, with frontal fault slip rates ranging from 70% to 130% of the deep convergence rate. For the fault system in Central Nepal, the periods when the frontal slip rate is lower than the deep loading rate are likely to feature more partial ruptures of the megathrust, leaving behind concentrated pockets of high stresses that affect the timing and slip of megathrust-spanning ruptures. In contrast, periods when the frontal slip rate is higher than the deep loading rate are likely to feature more frequent great ruptures that extend through the entire seismogenic zone.

Variable fault slip rates can cause local shortening rates to be measurably lower, comparable, or higher, than the deep loading rate depending on the history of internal deformation and the morphology of the underlying megathrust. Measurements of shortening from geodesy, which describe interseismic deformation over large regions, are representative of the long-term convergence rate between tectonic plates. This deformation is accommodated elastically around the deep regions of faults, and drives intermittent slip up-dip. In contrast, measurements with sensitivity to shallow deformation, such as geomorphic signals, incorporate the kinematics of the orogenic wedge.

Combining the kinematics of deep and shallow deformation allows a more comprehensive picture of the dynamics of a plate boundary, from the foreland to the hinterland. In Nepal, the deep convergence rate may also change with the life cycle of faults in the Tibetan Plateau and other changes in distant boundary conditions (Tapponnier et al., 2001; Wang and Barbot, 2023). These effects will be modulated by the internal deformation of the orogenic wedge, which impacts the local shortening most effectively near the frontal section.

CRediT authorship contribution statement

Sharadha Sathiakumar: Writing – review & editing, Writing – original draft, Visualization, Validation, Software, Resources, Methodology, Investigation, Formal analysis, Data curation, Conceptualization. Sylvain Barbot: Writing – review & editing, Writing – original draft, Supervision, Software, Project administration, Methodology, Investigation, Funding acquisition, Conceptualization. Judith Hubbard: Writing – review & editing, Writing – original draft, Supervision, Project administration, Methodology, Investigation, Funding acquisition, Formal analysis, Conceptualization.

Declaration of competing interest

The authors declare that they have no known competing financial interests or personal relationships that could have appeared to influence the work reported in this paper.

Data availability

The software code is publicly available at https://zenodo.org/record/4679513. The input scripts used to generate the data and figures can be found at https://doi.org/10.5281/zenodo.10634752. Additional data related to this paper may be requested from the authors.

Acknowledgements

This study is supported in part by the National Science Foundation under award number EAR-1848192. This study is also supported by the Earth Observatory of Singapore via its funding from the National Research Foundation Singapore and the Singapore Ministry of Education under the Research Centres of Excellence initiative.

Appendix A. Supplementary material

Supplementary material related to this article can be found online at https://doi.org/10.1016/j.epsl.2024.118599.

References

- Powell, C.M., Conaghan, P., 1973. Plate tectonics and the Himalayas. Earth Planet. Sci. Lett. 20 (1), 1–12.
- Molnar, P., Tapponnier, P., 1975. Cenozoic tectonics of Asia: effects of a continental collision: features of recent continental tectonics in Asia can be interpreted as results of the India-Eurasia collision. Science 189 (4201), 419–426.
- Tapponnier, P., Molnar, P., 1977. Active faulting and tectonics in China. J. Geophys. Res. 82 (20), 2905–2930. https://doi.org/10.1029/JB082i020p02905.
- Tapponnier, P., Peltzer, G., Armijo, R., 1986. On the mechanics of the collision between, India and Asia. Geol. Soc. (Lond.) Spec. Publ. 19 (1), 113–157. https://doi.org/10. 1144/GSL.SP.1986.019.01.07.
- Tapponnier, P., Zhiqin, X., Roger, F., Meyer, B., Arnaud, N., Wittlinger, G., Jingsui, Y., 2001. Oblique stepwise rise and growth of the Tibet Plateau. Science 294 (5547), 1671–1677.
- Avouac, J.-P., 2003. Mountain building, erosion, and the seismic cycle in the Nepal Himalaya. Adv. Geophys. 46, 1–80.
- Ding, L., Kapp, P., Cai, F., Garzione, C.N., Xiong, Z., Wang, H., Wang, C., 2022. Timing and mechanisms of Tibetan Plateau uplift. Nature Rev. Earth Environ., 1–16. https:// doi.org/10.1038/s43017-022-00318-4.
- Wang, L., Barbot, S., 2023. Three-dimensional kinematics of the India–Eurasia collision. Commun. Earth Environ. 4 (164). https://doi.org/10.1038/s43247-023-00815-4.
- Wesnousky, S.G., Kumar, S., Mohindra, R., Thakur, V., 1999. Uplift and convergence along the Himalayan frontal thrust of India. Tectonics 18 (6), 967–976.
- Yin, A., Harrison, T.M., 2000. Geologic evolution of the Himalayan-Tibetan orogen. Annu. Rev. Earth Planet. Sci. 28 (1), 211–280.
- Lavé, J., Avouac, J.-P., 2000. Active folding of fluvial terraces across the siwaliks hills, Himalayas of central Nepal. J. Geophys. Res. 105 (B3), 5735–5770.

- Lavé, J., Avouac, J.-P., 2001. Fluvial incision and tectonic uplift across the Himalayas of central Nepal. J. Geophys. Res., Solid Earth 106 (B11), 26561–26591.
- Hubbard, J., Almeida, R., Foster, A., Sapkota, S.N., Bürgi, P., Tapponnier, P., 2016. Structural segmentation controlled the 2015 Mw 7.8 Gorkha earthquake rupture in Nepal. Geology 44 (8), 639–642. https://doi.org/10.1130/G38077.1.
- Feldl, N., Bilham, R., 2006. Great Himalayan earthquakes and the Tibetan Plateau. Nature 444 (7116), 165–170.
- Bilham, R., 2019. Himalayan earthquakes: a review of historical seismicity and early 21st century slip potential. Geol. Soc. (Lond.) Spec. Publ. 483 (1), 423–482.
- Mugnier, J.-L., Gajurel, A., Huyghe, P., Jayangondaperumal, R., Jouanne, F., Upreti, B., 2013. Structural interpretation of the great earthquakes of the last millennium in the central Himalaya. Earth-Sci. Rev. 127, 30–47.
- Sapkota, S., Bollinger, L., Klinger, Y., Tapponnier, P., Gaudemer, Y., Tiwari, D., 2013.
 Primary surface ruptures of the great Himalayan earthquakes in 1934 and 1255. Nat. Geosci. 6 (1), 71–76.
- Gupta, H., Gahalaut, V., 2014. Seismotectonics and large earthquake generation in the Himalayan region. Gondwana Res. 25 (1), 204–213.
- Bollinger, L., Sapkota, S.N., Tapponnier, P., Klinger, Y., Rizza, M., Van der Woerd, J., Tiwari, D., Pandey, R., Bitri, A., Bes de Berc, S., 2014. Estimating the return times of great Himalayan earthquakes in eastern Nepal: evidence from the patu and bardibas strands of the main frontal thrust. J. Geophys. Res., Solid Earth 119 (9), 7123–7163.
- Qiu, Q., Hill, E.M., Barbot, S., Hubbard, J., Feng, W., Lindsey, E.O., Feng, L., Dai, K., Samsonov, S.V., Tapponnier, P., 2016. The mechanism of partial rupture of a locked megathrust: the role of fault morphology. Geology 44 (10), 875–878.
- Wesnousky, S.G., 2020. Great pending Himalaya earthquakes. Seismol. Res. Lett. 91 (6), 3334–3342.
- Masek, J.G., Duncan, C.C., 1998. Minimum-work mountain building. J. Geophys. Res., Solid Earth 103 (B1), 907–917.
- Dal Zilio, L., Hetényi, G., Hubbard, J., Bollinger, L., 2021. Building the Himalaya from tectonic to earthquake scales. Nature Rev. Earth Environ. 2 (4), 251–268.
- Lamb, S., 2021. The relation between short-and long-term deformation in actively deforming plate boundary zones. Philos. Trans. R. Soc. Lond. A 379 (2193), 20190414.
- Mallick, R., Bürgmann, R., Johnson, K., Hubbard, J., 2021. A unified framework for earthquake sequences and the growth of geological structure in fold-thrust belts. J. Geophys. Res., Solid Earth 126 (9), e2021JB022045.
- Suppe, J., 1983. Geometry and kinematics of fault-bend folding. Am. J. Sci. 283 (7), 684-721
- Qiu, Q., Barbot, S., 2022. Tsunami excitation in the outer wedge of global subduction zones. Earth-Sci. Rev., 104054. https://doi.org/10.1016/j.earscirev.2022.104054.
- Darwin, C., 1840. XLII.—On the connexion of certain volcanic phenomena in South America; and on the formation of mountain chains and volcanos, as the effect of the same power by which continents are elevated. Trans. Geol. Soc. Lond. 5 (3), 601–631.
- Van Dinther, Y., Gerya, T., Dalguer, L., Mai, P.M., Morra, G., Giardini, D., 2013. The seismic cycle at subduction thrusts: insights from seismo-thermo-mechanical models. J. Geophys. Res., Solid Earth 118 (12), 6183–6202.
- Van Zelst, I., Wollherr, S., Gabriel, A.-A., Madden, E.H., van Dinther, Y., 2019. Modeling megathrust earthquakes across scales: one-way coupling from geodynamics and seismic cycles to dynamic rupture. J. Geophys. Res., Solid Earth 124 (11), 11414–11446.
- Dal Zilio, L., van Dinther, Y., Gerya, T., Avouac, J.-P., 2019. Bimodal seismicity in the Himalaya controlled by fault friction and geometry. Nat. Commun. 10 (1), 48.
- Petrini, C., Gerya, T., Yarushina, V., van Dinther, Y., Connolly, J., Madonna, C., 2020. Seismo-hydro-mechanical modelling of the seismic cycle: methodology and implications for subduction zone seismicity. Tectonophysics 791, 228504.
- Uphoff, C., May, D.A., Gabriel, A.-A., 2023. A discontinuous Galerkin method for sequences of earthquakes and aseismic slip on multiple faults using unstructured curvilinear grids. Geophys. J. Int. 233 (1), 586–626. https://doi.org/10.1093/gji/ggac467.
- Hauck, M., Nelson, K., Brown, L., Zhao, W., Ross, A., 1998. Crustal structure of the Himalayan orogen at 90 east longitude from project indepth deep reflection profiles. Tectonics 17 (4), 481–500.
- Pandey, M., Tandukar, R., Avouac, J., Lave, J., Massot, J., 1995. Interseismic strain accumulation on the Himalayan crustal ramp (Nepal). Geophys. Res. Lett. 22 (7), 751–754
- Schelling, D., Arita, K., 1991. Thrust tectonics, crustal shortening, and the structure of the far-eastern Nepal Himalaya. Tectonics 10 (5), 851–862.
- Lemonnier, C., Marquis, G., Perrier, F., Avouac, J.-P., Chitrakar, G., Kafle, B., Sapkota, S., Gautam, U., Tiwari, D., Bano, M., 1999. Electrical structure of the Himalaya of central Nepal: high conductivity around the mid-crustal ramp along the mht. Geophys. Res. Lett. 26 (21), 3261–3264.
- Avouac, J.-P., Meng, L., Wei, S., Wang, T., Ampuero, J.-P., 2015. Lower edge of locked main Himalayan thrust unzipped by the 2015 gorkha earthquake. Nat. Geosci. 8 (9), 708–711.
- Bilham, R., 1995. Location and magnitude of the 1833 Nepal earthquake and its relation to the rupture zones of contiguous great Himalayan earthquakes. Curr. Sci. 69 (2), 101–128
- Bollinger, L., Tapponnier, P., Sapkota, S., Klinger, Y., 2016. Slip deficit in central Nepal: omen for a repeat of the 1344 ad earthquake? Earth Planets Space 68, 1–12.
- Pandey, M., Molnar, P., 1988. The distribution of intensity of the Bihar-Nepal earthquake of 15 January 1934 and bounds on the extent of the rupture zone. J. Nepal Geol. Soc. 5 (1), 22–44.
- Sathiakumar, S., Barbot, S., Hubbard, J., 2020. Earthquake cycles in fault-bend folds. J. Geophys. Res., Solid Earth 125 (8), e2019JB018557.

- Shaw, J.H., Connors, C.D., Suppe, J., et al., 2005. Seismic Interpretation of Contractional Fault-Related Folds: An AAPG Seismic Atlas, vol. 53. American Association of Petroleum Geologists.
- Barbot, S., 2019. Slow-slip, slow earthquakes, period-two cycles, full and partial ruptures, and deterministic chaos in a single asperity fault. Tectonophysics 768, 228171. https://doi.org/10.1016/j.tecto.2019.228171.
- Shi, Q., Barbot, S., Wei, S., Tapponnier, P., Matsuzawa, T., Shibazaki, B., 2020. Structural control and system-level behavior of the seismic cycle at the nankai trough. Earth Planets Space 72, 1–31.
- Barbot, S., 2020. Frictional and structural controls of seismic super-cycles at the Japan trench. Earth Planets Space 72 (1), 63.
- Sathiakumar, S., Barbot, S., 2021. The stop-start control of seismicity by fault bends along the main Himalayan thrust. Commun. Earth Environ. 2 (1), 1–11.
- Burbank, D.W., Leland, J., Fielding, E., Anderson, R.S., Brozovic, N., Reid, M.R., Duncan, C., 1996. Bedrock incision, rock uplift and threshold hillslopes in the northwestern Himalayas. Nature 379 (6565), 505–510.
- Godard, V., Bourlès, D.L., Spinabella, F., Burbank, D.W., Bookhagen, B., Fisher, G.B., Moulin, A., Léanni, L., 2014. Dominance of tectonics over climate in Himalayan denudation. Geology 42 (3), 243–246.
- Mishra, R.L., Singh, I., Pandey, A., Rao, P., Sahoo, H., Jayangondaperumal, R., 2016. Pale-oseismic evidence of a giant medieval earthquake in the eastern Himalaya. Geophys. Res. Lett. 43 (11), 5707–5715.
- Rajendran, C., Rajendran, K., 2021. Paleoseismic context of the 1950 earthquake: implications for seismic gaps in the eastern Himalaya. Phys. Chem. Earth Parts A/B/C 124, 103055.
- Ghoshal, S., McQuarrie, N., Robinson, D.M., Adhikari, D., Morgan, L.E., Ehlers, T.A., 2020.
 Constraining central Himalayan (Nepal) fault geometry through integrated thermochronology and thermokinematic modeling. Tectonics 39 (9), e2020TC006399.

- Lindsey, E.O., Almeida, R., Mallick, R., Hubbard, J., Bradley, K., Tsang, L.L., Liu, Y., Burgmann, R., Hill, E.M., 2018. Structural control on downdip locking extent of the Himalayan megathrust. J. Geophys. Res., Solid Earth 123 (6), 5265–5278.
- Li, S., Wang, Q., Yang, S., Qiao, X., Nie, Z., Zou, R., Ding, K., He, P., Chen, G., 2018. Geodetic imaging mega-thrust coupling beneath the Himalaya. Tectonophysics 747, 225–238.
- Stevens, V., Avouac, J., 2015. Interseismic coupling on the main Himalayan thrust. Geophys. Res. Lett. 42 (14), 5828–5837.
- Zheng, G., Wang, H., Wright, T.J., Lou, Y., Zhang, R., Zhang, W., Shi, C., Huang, J., Wei, N., 2017. Crustal deformation in the India-Eurasia collision zone from 25 years of gps measurements. J. Geophys. Res., Solid Earth 122 (11), 9290–9312.
- Hamahashi, M., Hubbard, J.A., Almeida, R.V., Haines, S.H., Owen, L.A., Mishra, S., Sapkota, S.N., 2022. Fluvial sedimentary response to late quaternary climate and tectonics at the Himalayan frontal thrust, central Nepal. Geochem. Geophys. Geosyst. 23 (9), e2022GC010366.
- Wesnousky, S.G., Kumahara, Y., Nakata, T., Chamlagain, D., Neupane, P., 2018. New observations disagree with previous interpretations of surface rupture along the Himalayan frontal thrust during the great 1934 Bihar-Nepal earthquake. Geophys. Res. Lett. 45 (6), 2652–2658.
- Rizza, M., Bollinger, L., Sapkota, S., Tapponnier, P., Klinger, Y., Karakaş, Ç., Kali, E., Etchebes, M., Tiwari, D., Siwakoti, I., et al., 2019. Post earthquake aggradation processes to hide surface ruptures in thrust systems: the m8. 3, 1934, Bihar-Nepal earthquake ruptures at Charnath Khola (Eastern Nepal). J. Geophys. Res., Solid Earth 124 (8), 9182–9207.
- Riesner, M., Bollinger, L., Rizza, M., Klinger, Y., Karakaş, Ç., Sapkota, S.N., Shah, C., Guérin, C., Tapponnier, P., 2023. Surface rupture and landscape response in the middle of the great mw 8.3 1934 earthquake mesoseismal area: Khutti khola site. Sci. Rep. 13 (1), 4566.